ICING CHARACTERISTICS ON NGCTR ENGINE INLET FOR RELEVANT CERTIFICATION CONDITIONS

Ellen Norde, ellen.norde@adse.eu, ADSE Consulting and Engineering (The Netherlands)
Stefan van 't Hoff, stefan.van.t.hoff@nlr.nl, Royal Netherlands Aerospace Centre NLR (The Netherlands)
Harmen van der Ven, harmen.van.der.ven@nlr.nl, Royal Netherlands Aerospace Centre NLR (The Netherlands)
Edwin van der Weide, e.t.a.vanderweide@utwente.nl, University of Twente (The Netherlands)
Ferdinand Spek, ferdinand.spek@adse.eu, ADSE Consulting and Engineering (The Netherlands)

Abstract

Rotorcraft engine air intakes are known to be particularly sensitive to inflight and ground icing and snow conditions. To allow early identification of geometrical features of the inlet that are sensitive to ice accumulation, the design can benefit from early icing analyses through numerical methods. This paper is focused on the icing assessment and optimisation of the engine intake duct of the Next Generation Civil Tilt Rotor (NGCTR) which is being developed by Leonardo Helicopters. Results for catching efficiency and water catch rates are presented for test cases that have been defined with respect to the operational envelope of the NGCTR and the requirements for atmospheric icing as defined in the EASA certification specifications for large aeroplanes, large rotorcraft and engines. It was found that both the water catch rate and the total water catch are lower for the NGCTR in conversion flight compared to the NGCTR in airplane flight conditions. Additionally, ground operations of the NGCTR are not found to be critical for icing in/on the engine inlet due to supercooled droplets.

1. INTRODUCTION

Civil tiltrotors cover the niche between traditional helicopters and fixed-wing aircraft. Their development is aimed at combining the operational advantages of both segments. Tiltrotor aircraft fly faster and further than conventional helicopters, while having vertical take-off and landing (VTOL) capabilities which fixed-wing aircraft do not feature.

Leonardo Helicopters is developing a Next Generation Civil Tilt Rotor (NGCTR) demonstrator within the EU Clean Sky 2 Fast Rotorcraft Programme [1]. The preliminary design of the NGCTR is focused on passenger transportation (~20 passengers) on short and medium flight distances up to 1000 nautical miles. The tiltrotor concept has a fixed engine installation with a split gearbox and a tiltable hub and rotor. Two aspects of this engine architecture are assessed within the TRINIDAT project: aerodynamic characteristics and icing effects. TRINIDAT is an acronym for Tilt Rotor INlet Innovative Design And Testing and the project consortium is represented by six partners: Royal Netherlands Aerospace Centre NLR, Deharde GmbH, Altran S.A.S. & Co. KG (now Capgemini Engineering), German-Dutch Wind Tunnels DNW, ADSE Consulting and Engineering and University of Twente [2]. An experimental evaluation of aerodynamic characteristics based on a wind tunnel test on a full-scale air intake model is presented in [3]. This paper covers the icing effects.

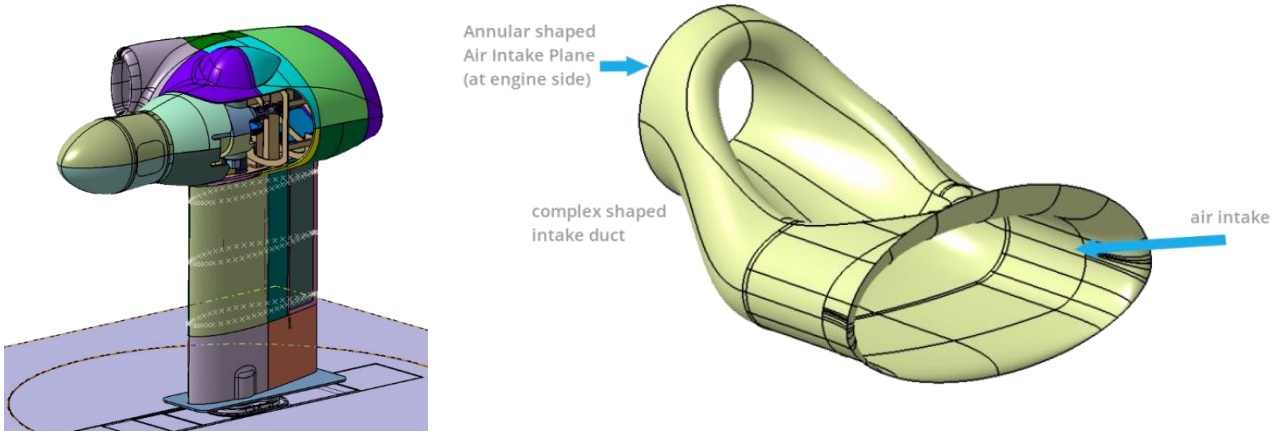

Figure 1 NGCTR engine intake configuration (left) and air intake duct (right)

Presented at 47th European Rotorcraft Forum, United Kingdom, 7-9th September, 2021

1.1. NGCTR Engine Configuration

The NGCTR engine intake configuration model and the intake duct are shown in Figure 1. The engine in fixed pitch position and the tiltable hub and rotor mounted at the wing tip. The engine air intake is followed by an S-shaped main intake duct which transitions into an annular air intake plane (AIP).

The engine configuration should ensure a highly efficient operation in aircraft mode as well as a proper operation during conversion and VTOL operations. As such, the shape of the intake duct should be optimised for maximum flow quality and minimal icing impact.

1.2. Objective

This paper is focused on the icing assessment of the NGCTR engine configuration. Rotorcraft engine air intakes are known to be particularly sensitive to inflight and ground icing conditions. Ice accumulation in/on the engine air intake, and ingestion of ice by the engine itself may cause a disturbance in the inlet aerodynamics which can cause surge, stall, flameout, or damage. Protective measures, such as electrothermal ice protection, inlet barrier filters, particle separators and/or inlet screens, are used on rotorcraft which are certified to operate in icing conditions. The air intake is designed to minimize the total pressure losses and achieve a uniform flow at the intake plane of the bare intake. To allow early identification of geometrical features of the inlet that are sensitive to ice accumulation, the design can benefit from early icing analyses through numerical methods as presented herein.

The objective of this paper is to illustrate the icing criticalities in terms of collection efficiency and water catch for the unprotected engine air intake of the NGCTR. Given the fact that the NGCTR split-gearbox configuration induces a radically different flow field around the engine air intake than conventional aircraft and existing tiltrotor aircraft, a thorough evaluation is needed to determine the critical flight and icing conditions for icing of the intakes and engines. These conditions are related to the flight envelope of the NGCTR and the applicable EASA Certification Specifications (CS). This paper presents the resulting catching efficiency and water catch rate for the test cases that have been defined with respect to supercooled droplet icing as defined in Appendix C of the EASA CS for large aeroplanes and large rotorcraft. No ice accretion analysis has been performed at this stage.

2. ICING CERTIFICATION

At this stage there is no clear understanding of the criticalities of the air intakes of the NGCTR configuration with its unique inlet geometry and with the conditions varying considerably between cruise and VTOL conditions. To provide early input for the ice protection system (IPS) development and certification, the existing certification requirements have been examined against the operational profile and flight envelope of the NGCTR. This has resulted in the selection of a number of icing conditions which have been analysed numerically.

2.1. Flight Envelope

Within the NGCTR flight envelope, three different modes of flight are considered:

- Aircraft cruise flight
- Conversion flight
- Helicopter (VTOL) and hover flight.

In aircraft mode the NGCTR has a cruise speed of ~300 knots at an altitude of 25,000 ft. In conversion and VTOL mode the maximum speed is ~140 knots, depending on the nacelle angle, at an altitude of 13,000 ft. The NGCTR is being designed to operate at ambient temperatures as cold as -45°C in all flight conditions. In normal operations the flight time in VTOL or conversion mode is short compared to the flight time in aircraft mode.

2.2. Certification Basis

For the development of the NGCTR the European airworthiness regulations are leading and, hence, the EASA certification specifications are the reference point. For icing certification the rules are a combination of fixed wing and rotorcraft regulation.

The EASA CS differentiate between normal (CS-23) and large (CS-25) category aeroplanes. Normal category aeroplanes have a passenger seating configuration of 19 or less and a maximum certified take-off mass of 8,618 kg (19,000 lbs). Since the NGCTR is a turbine powered large aeroplane, CS-25 [4] is applicable. If certification for flight in icing is sought, the aeroplane must at least be able to detect and safely exit Appendix O icing conditions in addition to being able to safely operate in Appendix C icing conditions. With respect to compliance it is stated in AMC25.1420 that: “Ice shapes to be tested are those representing the critical Appendix O icing conditions during recognition and subsequent exit from those icing conditions.” If, however, certification for (a portion) of Appendix O icing conditions is sought, it is likely that all freezing rain or all freezing drizzle conditions will be included. Within TRINIDAT it is currently assumed that operation in Appendix O icing conditions are out of scope and that the NGCTR will be equipped with suitable means to detect and safely exit these conditions.

Similarly, the EASA CS differentiate between small (CS-27) and large (CS-29) rotorcraft. Small rotorcraft have a maximum weight of 3,175 kg (7,000 lbs) and nine or less passenger seats. Since the NGCTR has a maximum weight greater than 9,072 kg (20,000 lbs) and 10 or more passenger seats it should be type certificated as large rotorcraft, Category A [5]. The AMC section of CS-29 refers to FAA guidance in AC29-2C [6] for icing certification. In AC29.1093(b)(1)(i) it is stated that the limited, i.e. less severe, icing envelopes described in AC29.1419 may be used to show compliance if the rotorcraft is limited to a maximum pressure altitude of 10,000 ft (3,048 m) for all operations. For the NGCTR this is not the case and, hence, the CS-29, Appendix C envelope must be used for operations in the altitude range up to 22,000 ft (6,706 m).

Finally, in CS-E 780 [7] it is stated that the engine should function satisfactorily when operated throughout the atmospheric icing conditions defined in the turbine engine's air intake system ice protection specifications. For the NGCTR those are CS-25.1093(b) and CS-29.1093(b), which have already been discussed above.

2.3. Icing Conditions

The icing conditions need to be selected such that the characteristics of the full atmospheric icing envelope are represented. These atmospheric icing conditions include:

- Continuous maximum (CM) icing (CS-25 / CS-29)
- Intermittent maximum (IM) icing (CS-25 / CS-29)
- Take-off maximum icing (CS-25)

Figure 2 shows the Appendix C icing envelopes and the NGCTR flight envelopes. It can be seen that the entire CM envelope and almost the entire IM envelope is within the airplane mode flight envelope. The CM and IM envelopes fall partly out of the VTOL/Conversion mode envelope.

In the scope of this study, the severity of icing conditions is related to the time in icing t_{ice} and the water catch rate, which is determined by the local catching efficiency β, the liquid water content LWC and the true airspeed V_{TAS}. The local total water catch TWC is thus given by:

$$TWC = \beta * LWC * V_{TAS} * t_{ice} \quad (1)$$

This dependency indicates that icing severity is high in particular flight phases:

- Holding: during holding the exposure time to icing conditions is long (45 minutes) and the LWC is high (no scaling for cloud extent)
- Cruise: during cruise the water catch rate is high when flying at maximum operating speed.

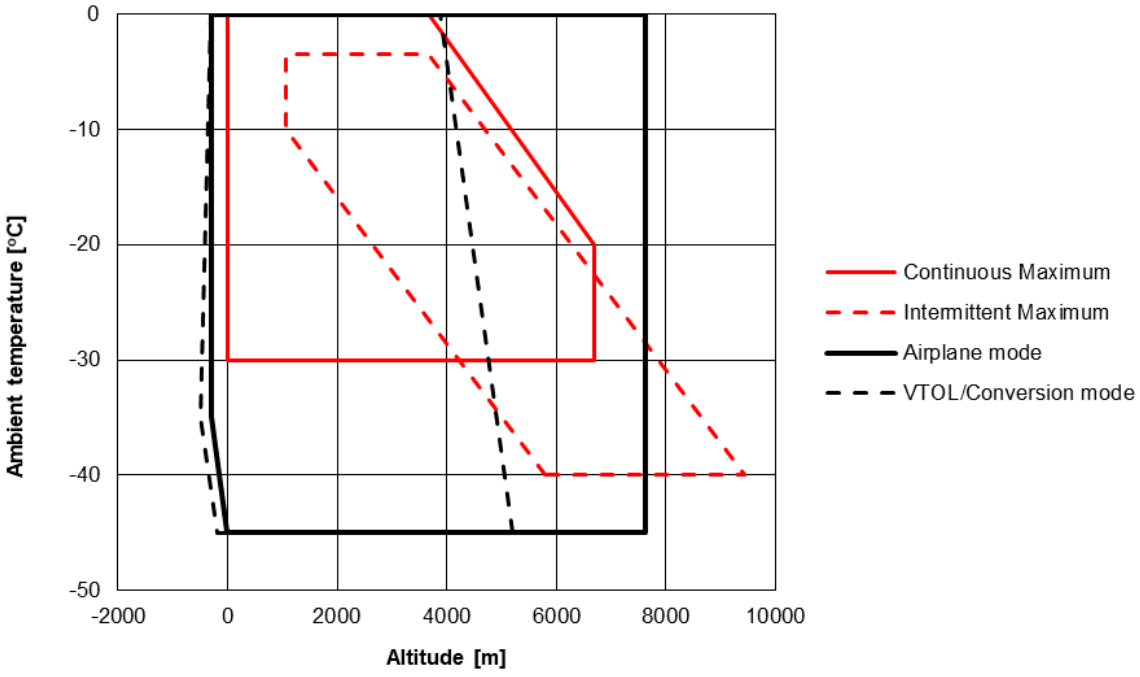

Figure 2 Appendix C icing envelope and NGCTR flight envelope

Table 1 Selected icing simulation conditions

ID	Flight condition	Engine mass flow	Nacelle [°]	V	PA [ft]	Cloud type	T [°C]	Icing time [min]
1	cruise	level flight	0	V_C	16,200	CM	-8.4	3.5
2	cruise	level flight	0	V_C	14,000	IM	-7.7	0.5
3	holding	level flight	0	V_H	13,500	CM	-3.0	45.0
4	holding	level flight	0	V_H	13,500	IM	-3.5	0.9
5	conversion	conversion flight	30	$V_{VTOL/30}$	12,900	CM	-1.7	0.5
6	conversion	conversion flight	30	$V_{VTOL/30}$	12,900	IM	-3.5	0.5
7	conversion	conversion flight	50	$V_{VTOL/50}$	12,600	CM	-1.2	20.0
8	conversion	conversion flight	50	$V_{VTOL/50}$	12,600	IM	-3.5	1.5
9	conversion	conversion flight	75	$V_{VTOL/75}$	12,200	CM	-0.5	20.0
10	conversion	conversion flight	75	$V_{VTOL/75}$	12,200	IM	-3.5	1.5
11	take-off	idle+TOP	90	0	0-1,500	n.a.	-9.0	1.0
12	ground ops	idle+TOP	90	0	0	n.a.	-9.0	>30.0

The relevant icing conditions have been determined for the cruise speed V_C and the holding speed V_H, as well as for conversion/VTOL velocities V_{VTOL} at nacelle angles 30°, 50° and 75°.

Furthermore, the LWC for atmospheric icing conditions increases with temperature. This indicates that the maximum LWC is obtained at an ambient temperature which results in a zero total air temperature (on non-rotating parts). Disregarding local effects, a total air temperature of zero is seen as the upper limit at which ice can accrete. A higher temperature also results in a higher true airspeed (TAS) for a constant equivalent airspeed (EAS). Hence, the maximum water catch temperature T and pressure altitude (PA) condition for a given EAS is found at the intercept of the CM/IM icing envelope boundary, given in Figure 2, with the flight condition for which the total air temperature equals zero. The ambient temperatures have been determined by setting the total temperature equal to 0 °C using a conservative assumption of a recovery factor of 70%. In case the flight condition falls out of the icing envelope, which is the case for holding and conversion flight with respect to the IM envelope, the ambient temperature is set to the maximum value of the considered icing envelope. It has been elected to include these IM conditions in the analysis, because IM icing is about three times more severe than CM icing in terms of LWC.

The icing time is either set by regulation, determined by the operational time of the flight condition, or is limited by the time it takes to fly straight through an icing cloud. For cruise conditions the icing time is given by the time it takes to fly through a standard CM cloud of 17.4 nautical miles horizontal extent and a standard IM cloud of 2.6 nautical miles horizontal extent at cruise speed. The icing time for the holding case in CM conditions is required to be 45 minutes by regulation. For conversion flight the icing time is determined by the operational time. This includes special operations such as search-and-rescue or loitering at nacelle angles of 50° and 75°. It is expected that these operations are not allowed when flying in IM conditions, but that in case of CM conditions the icing time is limited by the assumed maximum loitering duration of 20 minutes.

Finally, the ambient temperature range during take-off and ground operations and the icing time for ground operations are prescribed by the certification specifications. The icing time during take-off is determined by the time from lift-off to reach an altitude of 1,500 ft. Table 1 summarizes the flight and icing conditions which have been determined to be relevant for the NGCTR operational envelope.

3. SIMULATION METHOD

Numerical icing prediction codes are commonly used for droplet impingement limit analysis, IPS design and artificial ice shapes as required and recommended in CS-25. However, engine air intake design is typically driven by aerodynamic performance, with the sensitivity to flight in icing conditions being somewhat of an afterthought. Including icing analysis early in the design process reduces the risk of costly redesigns in the late development stages.

Over the years many droplet impingement and ice accretion codes for two- or three-dimensional bodies have been developed at universities, research institutes or industry for either internal or commercial use. In general, droplet impingement methods consist of an aerodynamic flow field computation (step 1) and a droplet trajectory and impingement calculation (step 2). For ice accretion methods these two steps are extended with a mass and thermodynamic balance computation (step 3) and an ice shape prediction (step 4). These calculations can be performed in a single step continuous process or in a multiple step iterative process.

The capabilities of an impingement or accretion code determine which specific analyses are best performed with it. If the focus is on (evaporative electrothermal) IPS design, then the code should be able to accurately predict the impingement limits and water catch. For ice shape determination, on the other hand, a code should be applied that has been compared and validated with ice shape results from inflight or wind tunnel experiments. With regard to ice accretion in a rotorcraft engine intake, many uncertainties exist and no extensive comparison with experimental data has been published in open literature. Therefore, it has been agreed with Leonardo Helicopters to focus the current study on impingement and water catch rate results rather than on ice accretion prediction. NLR and UT both have numerical methods available for solving droplet trajectories. The trajectory solver of NLR is named Trace and the trajectory solver of UT is named MooseMBIce. Details of the Trace solver are given in section 3.2 and details of the MooseMBIce solver are given in section 3.3.

3.1. Droplet Impingement

For droplet impingement analysis the following parameters are usually calculated:

- Impingement area and/or impingement limits
- Local water catch/collection efficiency β
- Total water catch rate $TWCR$

According to AMC 25.1419 the largest droplet diameter of the icing envelope should be used for determination of the impingement area/limits, while the full spectrum of droplet sizes should be considered in determining the water catch rates. Since the variation of droplet diameters in atmospheric clouds is high, a Langmuir distribution is generally used to represent the variation in Appendix C droplet diameters. In AC 20-73A [8] the Langmuir-D distribution is suggested for determining the impingement area/limits.

In numerical icing analyses the droplets are modelled as spheres. The droplet trajectories are calculated by taking into account the drag force and the gravitational force. The drag force depends on the velocity difference between the droplet and the airflow.

The local water catch efficiency β is defined as the ratio of droplet flux at the surface of impact relative to the droplet flux in the freestream. The total water catch rate $TWCR$, i.e. the amount of water that hits the surface per unit time, is determined by the surface integral over the (local) water catch rate (WCR):

$$TWCR = \int \beta * \mathrm{LWC} * V \ \mathrm{d}A \quad (2)$$

Where V is velocity, LWC is the liquid water content and A is the area of impingement, i.e. the frontal area of the object under investigation that is collecting droplets.

3.2. Trace

NLR's in-house general purpose Lagrangian particle trajectory solver Trace [9] is used herein for the prediction of the three-dimensional droplet trajectories, both as a pre-cursor computation for the analysis with MooseMBIce (see sections 3.3 and 3.4) and for the direct computation of the catching efficiency in the intake duct.

The particle trajectories are computed using the Lagrangian approach. The droplets are modelled as perfect spheres of a given diameter. Trace solves the three-degrees-of-freedom equations of motion. The equations of motion include both aerodynamic and inertial forces. For spherical particles the following analytic expression of the drag force is used [15]:

$$C_D = \begin{cases} \frac{24}{Re}(1 + 0.15Re^{0.687}) & \text{if } Re < 1000 \\ 0.44 & \text{otherwise} \end{cases} \quad (3)$$

The ordinary differential equations are integrated in time by an explicit four-stage Runge-Kutta scheme. For accuracy reasons, the time step is chosen such that a particle travels at most 1/12 mesh width within each time step.

3.3. MooseMBIce

UT's in-house method MooseMBIce is used to predict the droplet three-dimensional trajectories in the intake duct. MooseMBIce [10] has been developed and applied in the framework of EU-FP7 project HAIC (High Altitude Ice Crystals) [11]. The method also incorporates a prediction method for supercooled large droplets (SLD) [12] that has been developed separately in the framework of EU-FP7 project EXTICE (EXTreme ICing Environment) [13]. The particle trajectories are computed using the Eulerian approach. MooseMBIce employs a cell-centred finite-volume discretization with second-order spatial accuracy on multi-block structured grids. Time integration is performed by a standard low-storage four-stage Runge-Kutta scheme using local time stepping in order to obtain the particle trajectories. It has been assumed that the dispersed phase of particles is diluted within a continuous phase of air. In this case a one-way coupling with the air flow is sufficient to describe the particle trajectories accurately. MooseMBIce has been validated with experiments that have been executed within HAIC. The experiments have provided a strong validation basis since each part of the ice prediction method, i.e. trajectories, impingement, and accretion, have been validated separately.

3.4. Simulation Approach

To determine the criticality of the selected icing conditions given in Table 1, a simulation approach combining three different prediction methods has been adopted to compute the aerodynamic flow field (1), the droplet trajectories of the external domain of the inlet (2) and the droplet trajectories of the internal domain of the inlet (3).

The aerodynamic flow field is calculated by NLR's in-house CFD method ENFLOW. This method is an advanced CFD code suite with which steady or unsteady, incompressible or compressible flows around complex three-dimensional configurations have been simulated using RANS and hybrid RANS-LES models. The configurations can be either fixed or moving relative to an inertial reference frame, they can be either rigid or flexible, and they can consist of multiple bodies moving relative to one other, that fit suitably the NGCTR configuration. Since the design of an ice protection system for the nacelle inlet is out of the scope of the project, it has been agreed that a one-way, single step exchange between the aerodynamic solution and the icing prediction is sufficient. As part of the aerodynamic flow field generation, the parameters of the NGCTR configuration, i.e. engine mass flow ratio and the rotor performance data and blade motion, were matched as well as possible to a converging solution. The time-accurate aerodynamic flow results are obtained on a block-structured mesh with discontinuous interfaces which allow the blades to rotate and the rotor to tilt. The flow is averaged over a blade passing frequency to obtain a steady flow, which is input for the droplet analyses.

As MooseMBIce does not have the functionality for discontinuous interfaces, the MooseMBIce simulations have been performed within the inlet only, i.e. the internal domain (see section 3.4.2). Input for the MooseMBIce simulations on the inlet faces are obtained from Trace simulations on the external flow domain, i.e. external to the inlet (see section 3.4.1). As Trace will also be used to compute the catching efficiency in the inlet directly, the two approaches can be compared (see section 3.4.3). The solution on the inlet plane is exchanged between NLR and UT and more details on this analysis is given in section 3.4.3.

3.4.1. External Domain (Trace)

The droplet trajectories of the domain external to the engine inlet are computed with Trace. Given a steady flow field (time-averaged over a single blade revolution) the inlet is impacted by a multitude of spherical particles of a given diameter released well in front of the aircraft. Depending on the application, the location of the particles which hit the inlet face or the inlet duct are recorded. An unstructured quadrilateral mesh is constructed from the hit locations. From the face areas in this mesh the local catch efficiency is computed. The catch efficiency is then interpolated onto the inlet mesh used in the CFD computations. This allows to compute the catch efficiency for a distribution of particle diameters.

It has been observed that, given the complex 3-D flow field, particle trajectories cross one another. This undermines the basic assumption in the definition of the local catch efficiency β. The crossing of trajectories leads to folded and overlapping quadrilateral cells in the mesh of hit locations. The folded cells are removed from the mesh. As overlapping is not easily detected, unrealistic values of the local catch efficiency (>1) are ignored in the final determination of the catch efficiency.

The hit location area is, in general, not simply connected, even though the release area is. Any separate, connected areas are detected by removing high aspect ratio cells in the mesh of hit locations. The high aspect ratio cells have a relatively large area such that the catch efficiency is negligible anyway.

As the mesh of hit locations does not cover the complete inlet duct, some care must be taken in the interpolation. The mesh of hit locations is extended with those points in the CFD inlet mesh which are not covered by the hit mesh. At these locations, the catching efficiency is set to zero. The inverse-distance interpolation algorithm of Tecplot [16] is used for interpolation.

3.4.2. Internal Domain (MooseMBIce)

The droplet trajectories of the internal domain of the engine inlet are computed with MooseMBIce. MooseMBIce reads in the aerodynamic flow field in the interior domain and the local catch efficiencies at the inlet plane, provided by Trace, are set as a boundary condition

The droplets are modelled as spherical particles with a density that is equal to the density of water at 0°C. The droplet trajectories are computed with an Eulerian approach by solving the transport equations for volume fraction and momentum. In the momentum equation, source terms for drag, gravity and buoyancy are taken into account, while other forces on the droplet are assumed to be negligible. For computation of the drag force the drag coefficient expression from Langmuir and Blodgett is used [14], which is applicable for droplet Reynolds numbers below 1000 (in all applications the maximum Reynolds number of the droplets is significantly below this value):

$$C_D = \frac{24}{Re}(1 + 0.0197Re^{0.63} + 0.00026Re^{1.38}) \quad (4)$$

3.4.3. Inlet Plane Analysis

Underlying to the approach of separately computing the external and internal domain of the inlet is the assumption that the droplet characteristics at the inlet boundary can be captured by an inlet plane boundary condition. It is expected that the LWC field will be non-uniform and that LWC enhancement will occur, caused by rotor effects.

An inlet plane analysis has been performed and has shown the following:

- The droplet trajectories do not show a significant expansion or contraction.
- The LWC field at the inlet is asymmetric and reduced relative to the freestream.

These observations are visualised in Figure 3. This figure shows the droplet trajectories and the catching efficiency (β) field in the inlet plane for cruise (ID#1) and holding (ID#3) icing conditions for a droplet mean volumetric diameter MVD of 20 μm. Based on the inlet plane analysis it can be concluded that the suction effect of the engine is small for the in-flight conditions and that a large portion of the droplets will flow around the intake.

Furthermore, in order to verify the simulation approach, the combined Trace/MooseMBIce approach is compared with the direct Trace approach for the following two cases: cruise conditions (ID#1) for a droplet MVD of 20 μm and conversion conditions with a nacelle angle of 30 degrees (ID#5) for a droplet MVD of 40 μm.

Figure 4 shows the comparison of the catching efficiency for the cruise condition (ID-1 and ID-2) and a diameter of 20 micron. Differences can be seen at the rim of the inlet. These differences can be explained by the fact that in the Eulerian method the inflow of particles is assumed to be normal to the inlet face, which is not the case for the Lagrangian simulation (or in reality). Comparison is good in the more important, downstream, region of the inlet.

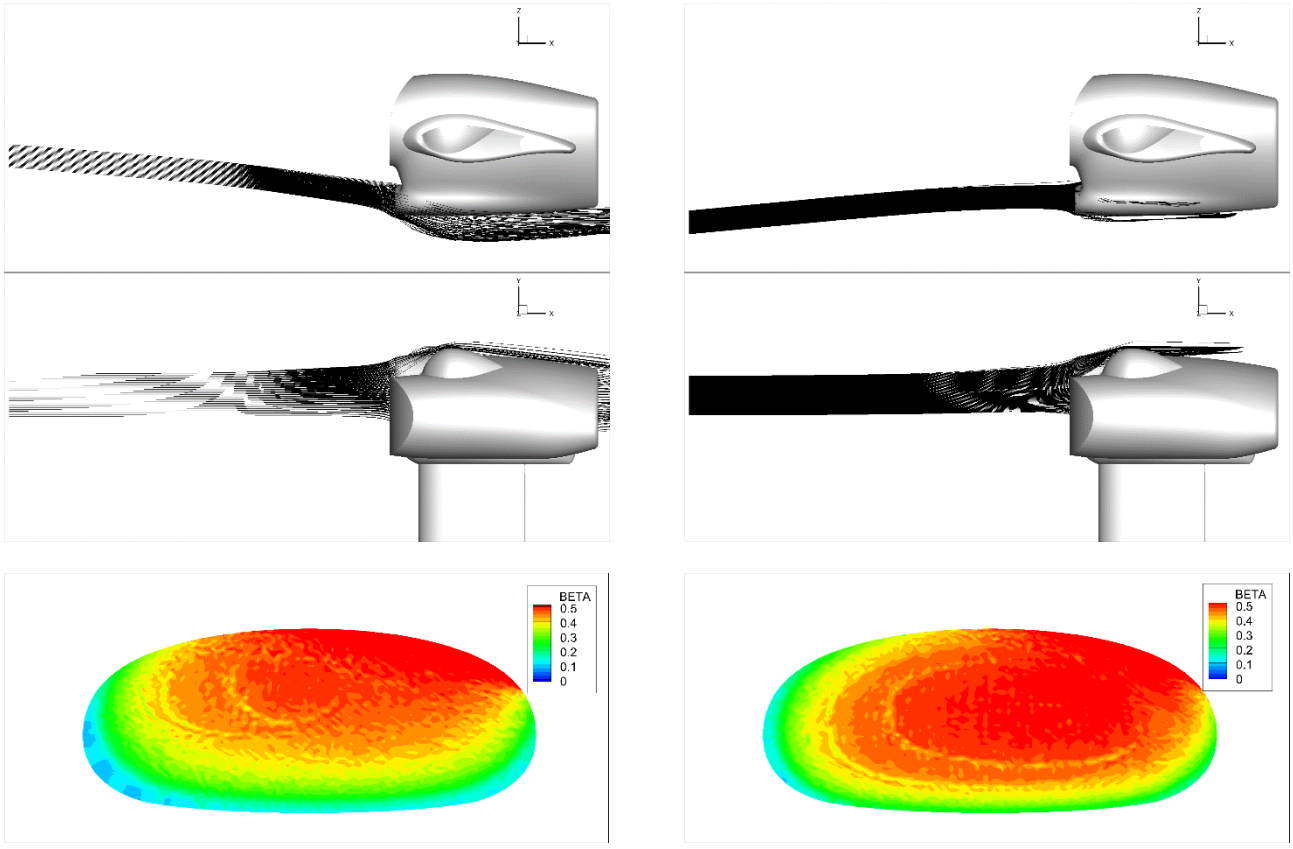

Figure 3 Droplet trajectories (top) and catching efficiency field inlet plane (bottom) for cruise condition ID#1 (left) and holding condition ID#3 (right)

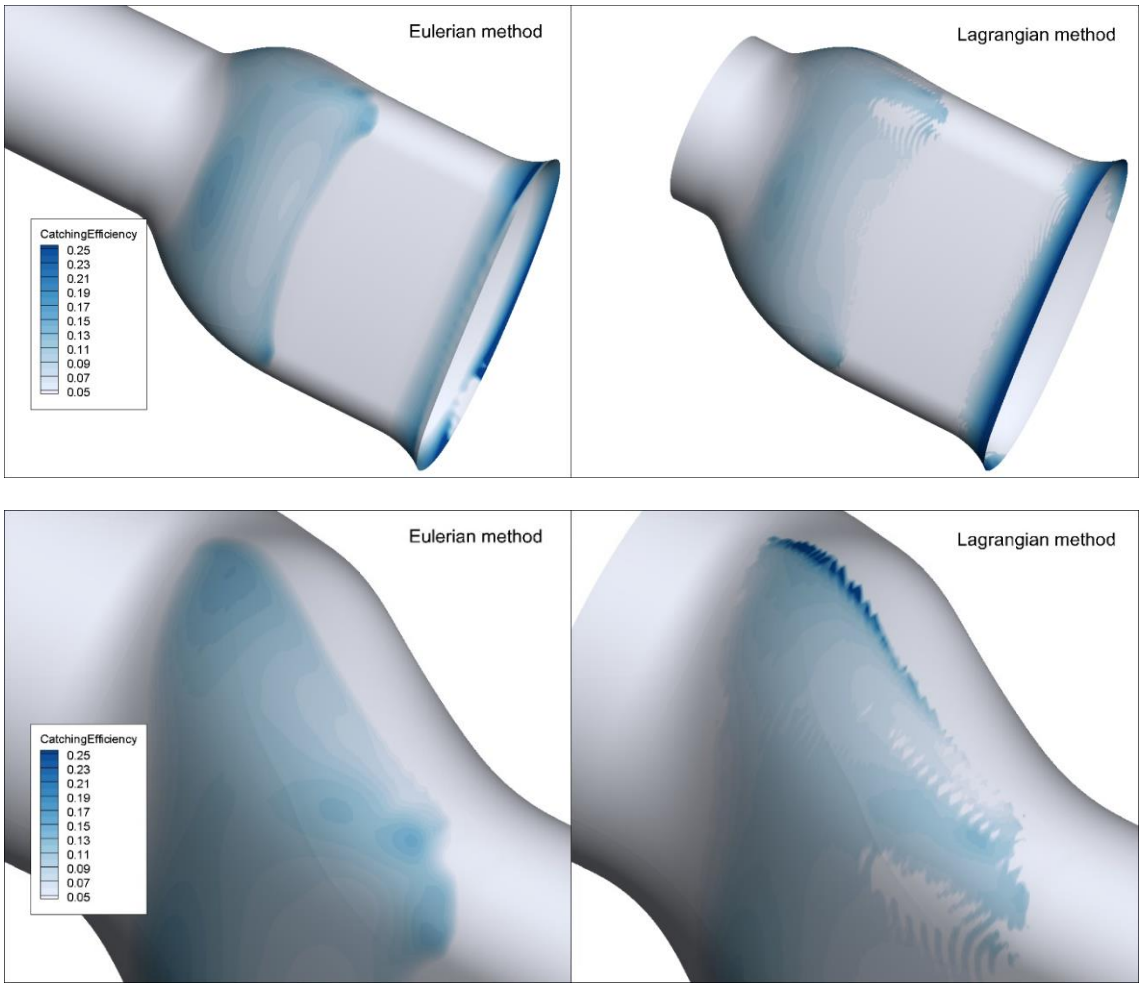

Figure 4 Catching efficiency field with MooseMBIce/Eulerian method (left) and Trace/Lagrangian method (right) for ID#1 with droplet MVD 20 µm, for complete inlet (top) and downstream region (bottom)

A detail of that specific region is shown in the bottom two plots of Figure 4. The presentation of the results from the Lagrangian approach suffers from crossing trajectories (resulting in high values of the catching efficiency at the top of the figure) and disconnected hit regions (resulting in the ragged regions to the right of the figure). The Eulerian approach presents a smoother image and reproduces the localized regions of higher catching efficiency at the start of the curvature of the inlet. In this respect, the combination of the Lagrangian and Eulerian method presents a more clear view of the catching efficiency.

This catching efficiency comparison has also been performed for ID#5. This comparison has again shown a good agreement between the results from the Lagrangian and Eulerian method in the downstream region of the inlet. Both methods display the highest catching efficiency just in front of the cylindrical section of the inlet. The difference being that the size of this region was slightly different and that the Lagrangian method showed more distortion due to crossing trajectories.

From the comparison it can be concluded that the combined Lagrangian/Eulerian approach is verified by the full Lagrangian approach, and that the LWC field can be set as an inlet plane boundary condition. Furthermore, the combined approach has the benefit of presenting a clearer image of the catching efficiency within the inlet.

4. RESULTS

This section summarizes the results of the impingement and water catch predictions for the selected icing conditions. The results for the inflight conditions are presented in section 4.1 and the results for the ground operations are presented in section 4.2.

4.1. Inflight Conditions

For the inflight conditions the critical droplet diameter is determined first, based on the results obtained with monodispersed droplet distributions. Based on the total water catch rates and amounts, three critical design conditions are selected for a more detailed water catch rate analysis. For these conditions the impingement and water catch prediction is repeated for a multi-dispersed Langmuir-D droplet distribution as is suggested in AC 20-73A. The LWC for the range of droplet sizes has been obtained by interpolating the LWC versus droplet size icing envelope for CM and IM clouds as given Appendix C of CS-25/CS-29 [4] [5].

The water catch rate WCR is defined as the amount of water that hits the surface per unit time. The total water catch rate has been obtained by integrating the water catch rate per unit area over the intake, see Equation (2). This results in the total water catch rate over the entire duct in grams per second. The highest total water catch rate has been observed for case ID#2, which is the highest velocity flight condition considered and corresponds to the cruise condition in an IM cloud. The total water catch rate for this case peaks at a droplet diameter of 20 μm.

When the maximum local water catch rates are compared, it is noticed that for the majority of the test cases a second peak is observed at a droplet diameter of 40 μm. This second peak is most distinctive for case ID#6, which corresponds to conversion flight at a nacelle angle of 30 degrees in an IM cloud. It should be noted that for the comparison of the maximum water catch rates the values near the inlet of the duct are ignored. As explained in section 3.4.1 unrealistically high values of the water catch rate were obtained for small droplets near the lip.

Finally, the total water catch has been determined for each case based on the derived icing time as given in Table 1. The highest total water catch is obtained for case ID#3, which corresponds to holding in CM conditions. In this condition, at a droplet diameter of 20 μm, the total water catch for the intake is estimated to be approximately five kilograms (based on single-step calculations of collection efficiency).

These three critical conditions, ID#2, ID#3 and ID#6, have been selected for further analysis. For these cases the water catch rate has been reassessed for a Langmuir-D distribution with an MVD equal to the critical diameter. The simulation conditions are given in Table 2. The results for each inflight conditions are discussed in the following sections.

4.1.1. Case ID#2

Case ID#2 corresponds to a cruise operation in an IM cloud. In Figure 5 the results for the water catch rates within the inlet are given for droplets with an MVD of 20 μm simulated with a Langmuir-D distribution (left figure) and with monodisperse distribution (right figure). It is observed that in both cases a high water catch exists in the lower middle region of the area before the duct transitions towards a circular shape. In that same area a second peak of the water catch rate is seen towards the left and right side just before the circular passage. For the monodisperse distribution this peak is seen at a more upward location (z-direction) compared to the Langmuir-D distribution. Furthermore, the areas with a high water impingement are less clearly defined for the Langmuir-D distribution compared to the monodisperse distribution. The maximum water catch rate and the total water catch rate are slightly higher for the Langmuir-D distribution compared to the monodisperse distribution. The reason for this is the relatively large contribution of the smaller droplets within the distribution due to their considerably large collection efficiency. The ratio (Langmuir-D/mono) for the maximum water catch rate is 1.059 and the ratio for the total water catch rate is 1.071. When the estimated icing time is taken into account this would result in a water catch of 0.41 kg in case of the Langmuir-D distribution.

Table 2 Critical icing simulation conditions

ID	Flight condition	Engine mass flow	Nacelle [°]	V	PA [ft]	Cloud type	T [°C]	t_{ice} [min]	d [μm]	LWC [g/m³]
2	cruise	level flight	0	V_C	14000	IM	-7.7	0.5	20 (MVD)	2.27
3	holding	level flight	0	V_H	13500	CM	-3.0	45.0	25 (MVD)	0.44
6	conversion	conversion flight	30	$V_{VTOL/30}$	12900	IM	-3.5	0.5	40 (MVD)	0.67
12	ground ops	idle+TOP	90	0	0	n.a.	-9.0	>30.0	20	0.30

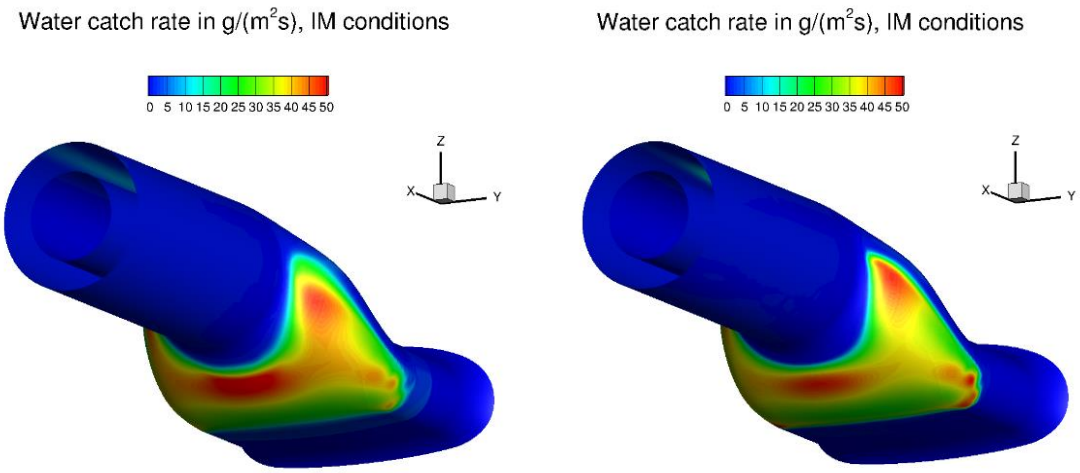

Figure 5 Water catch rate for ID#2 for a Langmuir-D distribution (left) and a monodisperse distribution (right)

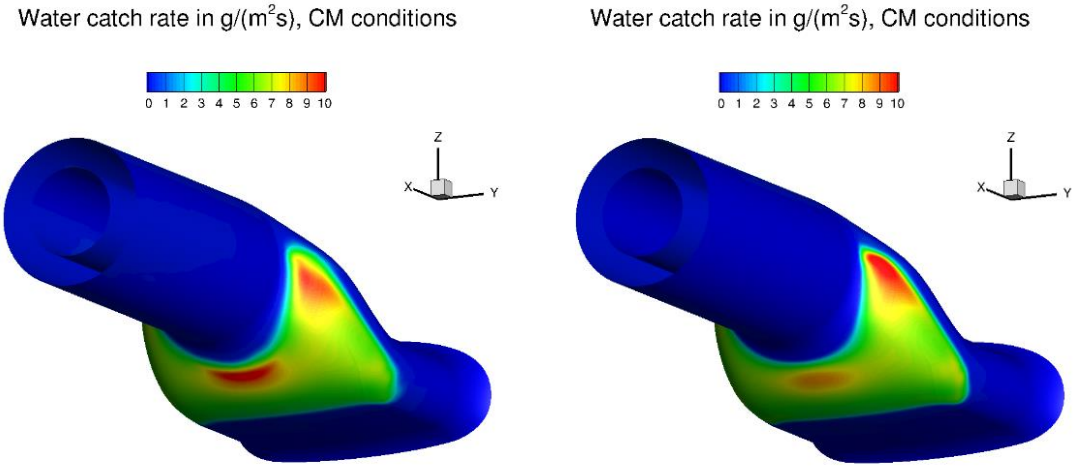

Figure 6 Water catch rate for ID#3 for a Langmuir-D distribution (left) and a monodisperse distribution (right). Note that the scale in this figure is different from the scale in Figure 5 and Figure 7.

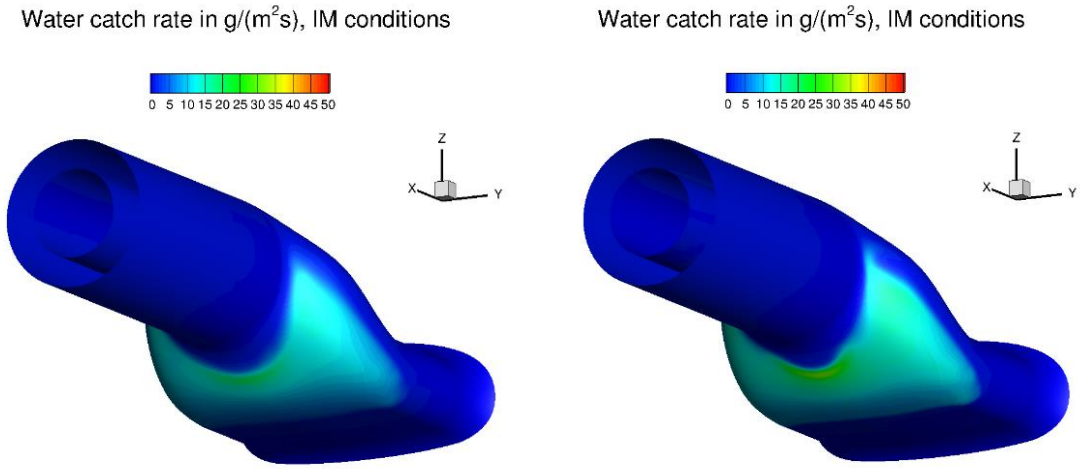

Figure 7 Water catch rate for ID#6 for a Langmuir-D distribution (left) and a monodisperse distribution (right)

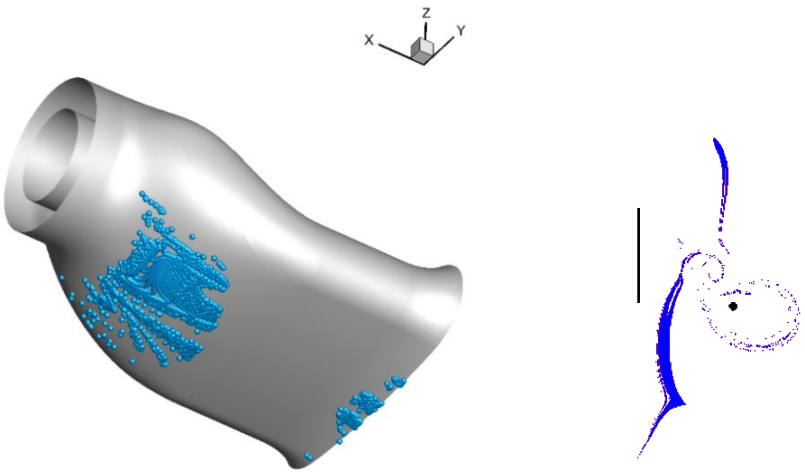

a) Particle hit locations

b) Particle release locations: in blue the particles which hit the inlet duct; the black line is the inlet face; the black dot the rotor center

Figure 8 Droplet impingement for ground operations

4.1.2. Case ID#3

Case ID#3 corresponds to a holding operation in a CM cloud. In Figure 6 the results for the water catch rates within the inlet are given for droplets with an MVD of 25 μm, simulated with a Langmuir-D distribution (left figure) and monodispersed (right figure). It is observed that for the Langmuir-D distribution the peak of the water catch rate shifts from the side towards the bottom region in the area before the transitioning to a circular shape when compared to the monodispersed solution. The maximum water catch rate and the total water catch rate are comparable for Langmuir-D distribution and the monodispersed cloud. The ratio for the maximum water catch rate is 0.981, where the monodispersed cloud has a slightly higher catch rate. The ratio for the total water catch rate is 1.055, where the Langmuir-D distribution has a slightly higher value. When the estimated icing time is taken into account this would result in a water catch of 5.15 kg in case of the Langmuir-D distribution.

4.1.3. Case ID#6

Case ID#6 corresponds to conversion mode operations at a nacelle angle of 30 degrees in an IM cloud. In Figure 7 the results for the water catch rates within the inlet are given for droplets with an MVD of 40 μm, simulated with a Langmuir-D distribution (left figure) and monodispersed (right figure). For this case a significant difference is observed between the two distributions. In both cases the highest water catch rate is seen in the lower middle region in the area before the duct transitions towards a circular shape. The peak of the maximum water catch rate that was seen for the monodisperse solution is, however, fairly flattened for the Langmuir-D distribution. Furthermore, the maximum water catch rate and the total water catch rate are higher for the monodispersed solution compared to the Langmuir-D distribution. The ratio (Langmuir-D/mono) for the maximum water catch rate is 0.665 and the ratio for the total water catch rate is 0.804. When the estimated icing time is taken into account this would result in a water catch of 0.09 kg in case of the Langmuir-D distribution.

4.2. Ground Operations

Ground icing was defined with the aircraft stationary in freezing fog conditions and (conservatively) with engine mass flow comparable to cruise conditions. For the ground operation case ID#12, see Figure 8, it is difficult to find starting positions of the droplets in the undisturbed flow: the droplets that are entering the inlet originate from a large upstream region. Moreover, the particle trajectories intersect with one another, making it impossible to define a catching efficiency. In an effort to investigate whether any droplets will enter the inlet, droplets are released from a horizontal plane about two meters above the rotor (i.e., in disturbed flow). The results are given in Figure 8. Figure 8a shows the hit locations. Figure 8b shows the particle release locations, where the particles that hit the inlet are shown in blue.

Figure 8b displays a complicated pattern and demonstrates why it is impossible to compute the catching efficiency. It can, however, be seen that out of the droplets released from an area of 4.5 m^2 immediately above the rotor, only around ~2.5% hit the inlet faces. In effect, the perpendicular orientation of the inlet relative to the rotor downwash, achieved by virtue of the split-gearbox operating concept, provides for a particle separator effect. Therefore, it would be safe to assume that for the NGCTR, ground operations are not critical for icing in/on the engine inlet due to supercooled droplets.

5. CONCLUSION AND OUTLOOK

Based on the results of the water catch rate analysis on the NGCTR engine inlet configuration in icing conditions it is concluded that:

- The highest water catch rate is obtained for the NGCTR in cruise for icing conditions representing an intermittent maximum (IM) cloud in airplane mode.
- The highest total water catch is obtained for the NGCTR in holding for icing conditions representing a continuous maximum (CM) cloud in airplane mode.
- In the interior domain of the inlet, two regions with a maximum water catch rate are observed:
    1. The lower middle region in the area where the duct transitions to a circular shape, referred to as the ‘chin’ of the duct.
    2. The left and right sides of the area where the duct transitions to a circular shape, referred to as the ‘cheeks’ of the duct.
- The ‘cheeks’ of the duct are more susceptible to impingement of smaller droplets, whereas the ‘chin’ of the duct is more susceptible to impingement of larger droplets.
- Both the water catch rate and the total water catch are lower for the NGCTR in conversion compared to the NGCTR in airplane flight conditions.
- Ground operations of the NGCTR are not critical for icing in/on the engine inlet due to supercooled droplets.

The assessment of the NGCTR engine inlet in icing conditions has shown that the critical area of droplet impingement exists near the small passage inside the inlet where the duct transitions towards a circular shape. It is expected that this region becomes less critical if the passage is widened and if the transition becomes smoother. These regions will be given special attention during the geometrical optimisation of the inlet which will be performed further on in the TRINIDAT project. The icing characteristics of the resulting inlet geometry will be assessed by means of a sensitivity analysis with respect to the baseline configuration.

6. ACKNOWLEDGEMENTS

This work was performed as part of the project TRINIDAT and has received funding from the Clean Sky 2 Joint Undertaking (JU) under grant agreement No 831810. The JU receives support from the European Union’s Horizon 2020 research and innovation programme and the Clean Sky 2 JU members other than the Union.

This paper reflects only the author’s view; the JU is not responsible for any use made of the information contained herein.

7. NOMENCLATURE

A	Area, [m^2]
β	Local water catch/collection efficiency, [-]
C_D	Drag coefficient, [-]
d	Diameter, [µm]
LWC	Liquid Water Content, [g/m^3]
MVD	Mean Volumetric Diameter, [µm]
Re	(Particle) Reynolds number, [-]
T	Temperature, [°C]
t_{ice}	Icing time, [s]
TWC	Total Water Catch, [g/m^2]
$TWCR$	Total Water Catch Rate, [g/s]
V	Velocity, [m/s]
WCR	Water Catch Rate, [g/(m^{2}s)]

8. GLOSSARY

AC	Advisory Circular
AIP	Air Intake Plane
AMC	Acceptable Means of Compliance
CM	Continuous Maximum
CS	Certification Specifications
EAS	Equivalent Airspeed
EASA	European Aviation Safety Agency
EXTICE	EXTreme ICing Environment
FAA	Federal Aviation Administration
HAIC	High Altitude Ice Crystals
IM	Intermittent Maximum
IPS	Ice Protection System
NGCTR	Next Generation Civil Tilt Rotor
PA	Pressure Altitude
SLD	Supercooled Large Droplets
TAS	True Airspeed
VTOL	Vertical Take-Off and Landing

9. REFERENCES

[1] Horizon 2020, Clean Sky 2, Fast Rotorcraft IADP, cleansky.eu/fast-rotorcraft-iadp, visited 8 June 2021

[2] Horizon 2020, Clean Sky 2, TRINIDAT project, GA no. 831810, project.nlr.nl/trinidat, visited 8 June 2021

[3] Habing, R., Philipsen, I., Müller, M., Pecoraro, M., "Experimental Evaluation Of Flow Distortion At Tilt-Rotor Full-Scale Model Air Intake Wind Tunnel Test", 47th ERF, paper 20, 2021

[4] EASA, Certification Specifications and Acceptable Means of Compliance for Large Aeroplanes CS-25 Amendment 26, 15 December 2020

[5] EASA, Certification Specifications and Acceptable Means of Compliance for Large Rotorcraft CS-29 Amendment 8, 24 June 2020

[6] FAA Advisory Circular AC 29-2C, Certification of Normal Category Rotorcraft, 2 July 2018, Change 8

[7] EASA, Certification Specifications and Acceptable Means of Compliance for Engines CS-E Amendment 6, 24 June 2020

[8] FAA Advisory Circular AC 20-73A, Aircraft Ice Protection, 16 August 2006

[9] Muijden, J. van, Laban, M., and Kok, J.C., "Icing tunnel flow quality and test section liquid water content distribution", CFD data, NLR-CR-98490, 1998

[10] Norde, E., "Eulerian method for ice crystal icing in turbofan engines", PhD Thesis, University of Twente, 11 May 2017

[11] European Commission, High Altitude Ice Crystals, cordis.europa.eu/project/id/314314, visited 8 June 2021

[12] Hospers, J.M., "Eulerian method for super-cooled large-droplet ice-accretion on aircraft wings", PhD Thesis, University of Twente, 27 November 2013

[13] European Commission, EXTreme ICing Environment, cordis.europa.eu/project/id/211927, visited 8 June 2021

[14] Langmuir, I., and Blodgett, K.B., "A mathematical investigation of water droplet trajectories", Technical Report 5418, US Army Air Forces, 1946

[15] D. Gidaspow, Multiphase Flow and Fluidization: Continuum and Kinetic Theory Descriptions, Academic Press, 1994

[16] Tecplot CFD visualization and analysis tools, tecplot.com